Molecular Therapy
Original Article

Genetic Rescue Reverses Microglial Activation in Preclinical Models of Retinitis Pigmentosa

Lijuan Zhang,[1,11] Xuan Cui,[2,3,4,5,11] Ruben Jauregui,[3,4,6] Karen Sophia Park,[3,4] Sally Justus,[3,4,7] Yi-Ting Tsai,[3,4] Jimmy K. Duong,[8] Chun-Wei Hsu,[3,4] Wen-Hsuan Wu,[3,4] Christine L. Xu,[3,4] Chyuan-Sheng Lin,[9] and Stephen H. Tsang[3,4,10]

[1]Shanxi Eye Hospital, affiliated with Shanxi Medical University, 100 Fudong St., Xinghualing, Taiyuan, Shanxi, China; [2]Tianjin Medical University Eye Hospital, Tianjin Medical University Eye Institute & Tianjin Medical University School of Optometry and Ophthalmology, Tianjin 300384, China; [3]Jonas Children's Vision Care and the Bernard & Shirlee Brown Glaucoma Laboratory, Department of Ophthalmology, Columbia Stem Cell Initiative, Columbia University, New York, NY, USA; [4]Edward S. Harkness Eye Institute, New York-Presbyterian Hospital, New York, NY, USA; [5]Tianjin Medical University Eye Hospital, Tianjin, China; [6]Weill Cornell Medical College, New York, NY, USA; [7]Harvard Medical School, Boston, MA, USA; [8]Department of Biostatistics, Mailman School of Public Health, Columbia University Medical Center, New York, NY, USA; [9]Department of Pathology and Cell Biology, Herbert Irving Comprehensive Cancer Center, College of Physicians and Surgeons, Columbia University Medical Center, New York, NY, USA; [10]Department of Pathology & Cell Biology, Stem Cell Initiative (CSCI), Institute of Human Nutrition, College of Physicians and Surgeons, Columbia University, New York, NY, USA

Microglia cells (MGCs) play a key role in scavenging pathogens and phagocytosing cellular debris in the central nervous system and retina. Their activation, however, contributes to the progression of multiple degenerative diseases. Given the potential damage created by MGCs, it is important to better understand their mechanism of activation. Here, we explored the role of MGCs in the context of retinitis pigmentosa (RP) by using four independent preclinical mouse models. For therapeutic modeling, tamoxifen-inducible CreER was introduced to explore changes in MGCs when RP progression halted. The phenotypes of the MGCs were observed using live optical coherence tomography, live autofluorescence, and immunohistochemistry. We found that, regardless of genetic background, MGCs were activated in neurodegenerative conditions and migrated beyond the layers where they are typically found to the inner and outer segments, where degeneration was ongoing. Genetic rescue not only halted degeneration but also deactivated MGCs, regardless of whether the intervention occurred at the early, middle, or late stage of the disease. These findings suggest that halting long-term disease progression may be more successful by downregulating MGC activity while co-administering the therapeutic intervention.

INTRODUCTION

Microglia cells (MGCs) are a specialized type of resident macrophage that have been described as the sentinels of the CNS for their role in scavenging pathogens and phagocytosing cellular debris.[1] MGCs are distinguished from other glial cells, such as astrocytes and oligodendrocytes, through their origin, gene expression pattern, morphology, and functions.[2,3] It is believed that MGCs are derived from primitive hematopoiesis in the fetal yolk sac and function as the resident immune cells in the CNS and retina.[4] MGCs are highly sensitive to their environmental milieu and remain quiescent until activated, as they are primarily recruited in response to subtle changes resulting from the compromise of the physiological integrity of other cells.[5] Once activated, they perform two primary functions: phagocytose debris from the site of injury and release inflammatory mediators into the extracellular space.[6–8]

Activation of MGCs has been shown to contribute to disease progression in multiple CNS diseases, such as stroke, Parkinson's disease, and Alzheimer's disease.[9–11] In a stroke, for example, activated MGCs phagocytose debris from the primary injury site and secrete molecules that kill nearby unaffected neurons. Similarly, we suggest that MGCs are activated by primary rod cell death and in addition may kill adjacent photoreceptors.[12] An analogous phenomenon has been observed in the retina, where exaggerated, chronic MGC reactions are suspected to contribute to photoreceptor degeneration.[1,12] Recent studies have found that activated retinal MGCs contribute to photoreceptor death via phagocytic activation and production of pro-inflammatory factors. In a study of retinal degenerative conditions, specifically late-onset retinal degeneration, age-related macular degeneration, and retinitis pigmentosa (RP), MGCs were greater in number compared to controls and stained positively for markers of rod photoreceptors.[12] Thus, while MGCs play an important role in cell protection against pathogens and other insults, they can also cause harm by promoting neuroinflammation, which is cytotoxic and induces death in

Received 14 February 2018; accepted 15 June 2018;
https://doi.org/10.1016/j.ymthe.2018.06.014.

[11]These authors contributed equally to this work.

Correspondence: Stephen H. Tsang, MD, PhD, Edward S. Harkness Eye Institute, New York-Presbyterian Hospital/Columbia University Irving Medical Center, 635 West 165th Street, Box 112, New York, NY 10032, USA.
E-mail: sht2@columbia.edu
Correspondence: Lijuan Zhang, MD, PhD, Shanxi Eye Hospital, affiliated with Shanxi Medical University, 100 Fudong St., Xinghualing, Taiyuan, Shanxi, China.
E-mail: zhanglj2004@163.com

neighboring cells.[12] Here, we further explore MGC activation in the context of RP.

RP is a group of inherited retinal degenerative conditions that present with photoreceptor death. It has been estimated that 1 in 4,000 are affected by RP, a disease that significantly impairs the ability to conduct activities of daily living and leads to a substantial public health burden.[13] RP patients initially present with symptoms such as difficulty seeing at night, peripheral vision deterioration, development of tunnel vision, and eventual blindness.[14–16] Although gene therapy holds potential as a novel strategy for slowing or even halting disease progression, there is currently no treatment for RP. One of the challenges in treating RP using gene therapy is the disease's genetic heterogeneity, as there are more than 60 genes associated with RP. Gene therapy approaches are specific to the affected gene, thus limiting the scalability and clinical relevance of this treatment modality. In most forms of RP, the mutations are expressed in rod photoreceptors, but cone photoreceptor death also occurs.[17] The mechanism behind secondary cone death, however, remains a mystery. Thus, developing a mechanism that prevents disease progression, regardless of the affected gene, is an important unmet need for treating inherited conditions like RP.

Mutations in rod phosphodiesterase (*Pde6*) contribute to approximately 4% of autosomal recessive RP (arRP) cases.[18,19] The rod PDE6 protein is composed of two catalytic subunits, Pde6-alpha (PDE6A) and Pde6-beta (PDE6B) and a pair of inhibitory Pde6-gamma (PDE6G) subunits. Mutations in *Pde6* prevent the photoexcitation cascade from functioning properly, in addition to causing primary rod cell death through elevated cyclic guanosine monophosphate (cGMP) levels, unregulated influx of calcium, and subsequent secondary cone loss.[20,21] In this study, we analyzed four different rod *Pde6*-associated mouse models of RP: $Pde6a^{D670G/D670G}$, $Pde6b^{H620Q/H620Q}$, $Pde6b^{STOP/STOP}$, and $Pde6b^{H620Q/STOP}$. $Pde6a^{D670G/D670G}$, which involves an aspartic acid-to-glycine residue conversion at amino acid 670, presents the most advanced phenotype, with overt morphological changes detectable by 1 week postnatally and complete retinal degeneration by 4 weeks. $Pde6b^{H620Q/H620Q}$ mice possess a histidine-to-glutamine residue conversion at amino acid 620 in the PDE6b subunit, inducing the mildest phenotype of the three models. Retinal degeneration in this mouse model is observable around 2 weeks postnatally and is complete by 8 to 10 weeks.[22,23] $Pde6b^{STOP/STOP}$ is a new genetic model of RP that carries a floxed STOP cassette in intron one of each *Pde6b* allele, preventing PDE6B from being expressed in the absence of Cre recombinase activity.[24,25] Each of the mouse models described above was labeled with GFP at the CX3CR1 receptor. Thus, the genotype of each mouse is $Pde6a^{D670G/D670G}$;$Cx3cr1\text{-}GFP^{+/-}$, $Pde6b^{H620Q/H620Q}$;$Cx3cr1\text{-}GFP^{+/-}$, $Pde6b^{STOP/STOP}$;$Cx3cr1\text{-}GFP^{+/-}$, and $Pde6b^{H620Q/STOP}$;$Cx3cr1\text{-}GFP^{+/-}$; hereafter they will be referred to as $Pde6a^{D670G/D670G}$, $Pde6b^{H620Q/H620Q}$, $Pde6b^{STOP/STOP}$, and $Pde6b^{H620Q/STOP}$, respectively. CX3CR1 is a delta chemokine receptor that is specifically expressed in MGCs and their neuronal ligand.[26,27] It has been widely studied previously in the context of the CNS,[28,29] liver,[30] intestinal system,[31] and skeletal muscles.[32] $Cx3xr1^{GFP/GFP}$ and $Cx3xr1^{GFP/+}$ mouse models were commonly used to conduct the aforementioned studies. *Cx3cr1::GFP* can be observed in both live and fixed tissue, although most research done so far has focused on the latter.

In this study, we present one of the first characterizations of the effects of neurodegeneration on MGC activation in the retina via the CX3CR1 receptor in living mice with retinal degeneration caused by a *Pde6* mutation. We also halted degeneration at early, middle, and late disease stages with genetic rescue and assessed the effects on the MGC population, providing a new paradigm for the study of MGCs in neurodegeneration and retinal degenerative diseases.

RESULTS

MGCs Are Activated in Multiple Preclinical Models of RP

Optical coherence tomography (OCT) imaging, which provides live cross-sectional images through the retina, was performed on mutant mice ($Pde6b^{STOP/STOP}$, $Pde6b^{H620Q/H620Q}$, and $Pde6a^{D670G/D670G}$), and age-matched WT ($Pde6b^{H620Q/+}$;$Cx3cr1\text{-}GFP^{+/-}$) mice at 4 weeks (Figure 1A). Diminished outer retinal layer thickness was exhibited in all three RP models compared to WT. Photoreceptor thickness obtained with OCT was quantified and presented graphically, showing a significant difference ($p < 0.001$) for all three mutant groups compared to WT (Figure 1C). A statistically significant difference in photoreceptor thickness was found between $Pde6a^{D670G/D670G}$ and $Pde6b^{H620Q/H620Q}$ ($p < 0.001$) as well as between $Pde6a^{D670G/D670G}$ and $Pde6b^{STOP/STOP}$ ($p < 0.001$), while no difference was found between $Pde6b^{STOP/STOP}$ and $Pde6b^{H620Q/H620Q}$. $Pde6a^{D670G/D670G}$ showed the most severe phenotype, as it displayed the thinnest layers on OCT compared to the other two mutant models at the same age.

A confocal scanning laser ophthalmoscope (cSLO) was used to perform SLO imaging on the three mutant mouse models and WT mice at 4 weeks postnatally (Figure 1B). GFP, which was expressed under the control of the *Cx3cr1* promoter, served as a reporter of the density of live MGCs in all WT and mutant mice. A higher density of MGCs was found in all three mutant mice compared to WT (Figure 1D). Statistically significant differences were found in all mutant mice compared to WT: $p = 0.004$ for $Pde6b^{H620Q/H620Q}$; $p < 0.001$ for $Pde6b^{STOP/STOP}$; $p < 0.001$ for $Pde6a^{D670G/D670G}$. Notably, there was also a significant difference in MGC density between each mutant mouse model: $Pde6b^{H620Q/H620Q}$ versus $Pde6b^{STOP/STOP}$ ($p = 0.002$); $Pde6b^{H620Q/H620Q}$ versus $Pde6a^{D670G/D670G}$ ($p = 0.02$); $Pde6b^{STOP/STOP}$ versus $Pde6a^{D670G/D670G}$ ($p < 0.001$). The $Pde6a^{D670G/D670G}$ mice, which had the lowest MGC density compared to the other *Pde6b* mutant mice, showed MGCs congregating to form denser areas, which were not observed in the other mutants. Based on our observation, the denser patches were randomly distributed throughout the retina except in the peripapillary area, where a particularly higher density of MGCs was observed. Although the $Pde6a^{D670G/D670G}$ mouse model exhibited the lowest MGC density despite displaying the severest degenerative phenotype, we believe that the low density may result from the fact that there is very minimal ONL remaining at this stage in this particular model.

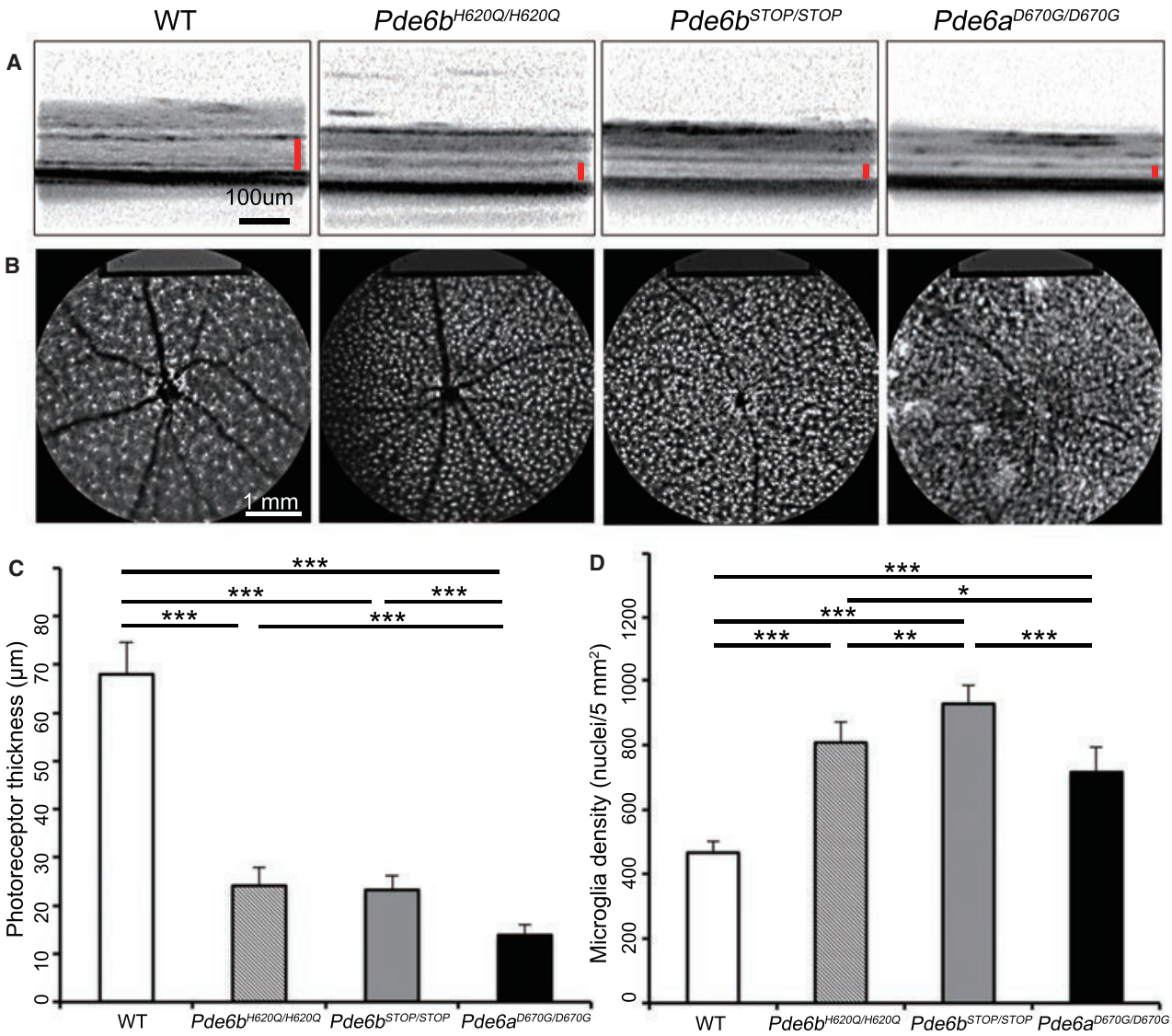

Figure 1. MGC Aggregation Is Directly Proportional to Disease Severity of Preclinical Models

(A) Live OCT images were taken from three mutant mouse models (*Pde6b*$^{H620Q/H620Q}$, *Pde6b*$^{STOP/STOP}$, and *Pde6a*$^{D670G/D670G}$) at 4 weeks as compared to WT, with the red bar indicating the ONL and IS/OS layers (scale bar, 100 μm). (B) Live SLO images were taken from WT and three mutant mouse models at 4 weeks. The white dots, obtained by cSLO, are GFP expressed under the control of the *Cx3cr1* promoter in MGCs (scale bar, 1 mm). (C) Photoreceptor thickness was measured and quantified based on OCT images from WT and mutant mice. $p < 0.001$ for WT compared to all three mutant groups; $p < 0.001$ for *Pde6a*$^{D670G/D670G}$ compared to *Pde6b*$^{H620Q/H620Q}$ and *Pde6b*$^{STOP/STOP}$. For WT, n = 10 eyes. For all mutant groups, n = 8 eyes. (D) The MGC density was captured using SLO at 4 weeks and measured and quantified by ImageJ in WT and mutant mice. $p = 0.004$ between WT and *Pde6b*$^{H620Q/H620Q}$; $p < 0.001$ for WT compared to *Pde6b*$^{STOP/STOP}$ and *Pde6a*$^{D670G/D670G}$. $p = 0.002$ between *Pde6b*$^{H620Q/H620Q}$ and *Pde6b*$^{STOP/STOP}$; $p = 0.02$ between *Pde6b*$^{H620Q/H620Q}$ and *Pde6a*$^{D670G/D670G}$; $p < 0.001$ between *Pde6b*$^{STOP/STOP}$ and *Pde6a*$^{D670G/D670G}$. For WT, n = 10 eyes. For all mutant groups, n = 8 eyes. OCT, optical coherence tomography; ONL, outer nuclear layer; IS/OS, inner and outer segment layers; cSLO, confocal scanning laser ophthalmoscope. *$p < 0.05$; **$p < 0.01$; ***$p < 0.001$. Error bars are 1 SD.

MGCs Migrate to the Sites Where Degeneration Occurs, Especially to the IS/OS Layers and ONL

Vertical retinal sections were collected at 3, 6, and 12 weeks from WT (*Pde6b*$^{H620Q/+}$;*Cx3cr1-GFP*$^{+/-}$) mice (Figures 2A, 2E, and 2I), *Pde6b*$^{STOP/STOP}$ (Figures 2B, 2F, and 2J), *Pde6b*$^{H620Q/H620Q}$ (Figures 2C, 2G, and 2K), and *Pde6a*$^{D670G/D670G}$ (Figures 2D, 2H, and 2L). Sections were stained for GFP, which is co-localized to MGCs under the control of the *Cx3cr1* promoter.[33] The thickness of the ONL was stable in WT mice, while an apparent decrease of the ONL thickness was detected in the time period from 3 to 6 weeks, with roughly only one row of photoreceptors remaining in the ONL at 12 weeks for all three RP models. When there was no retinal degeneration, MGCs

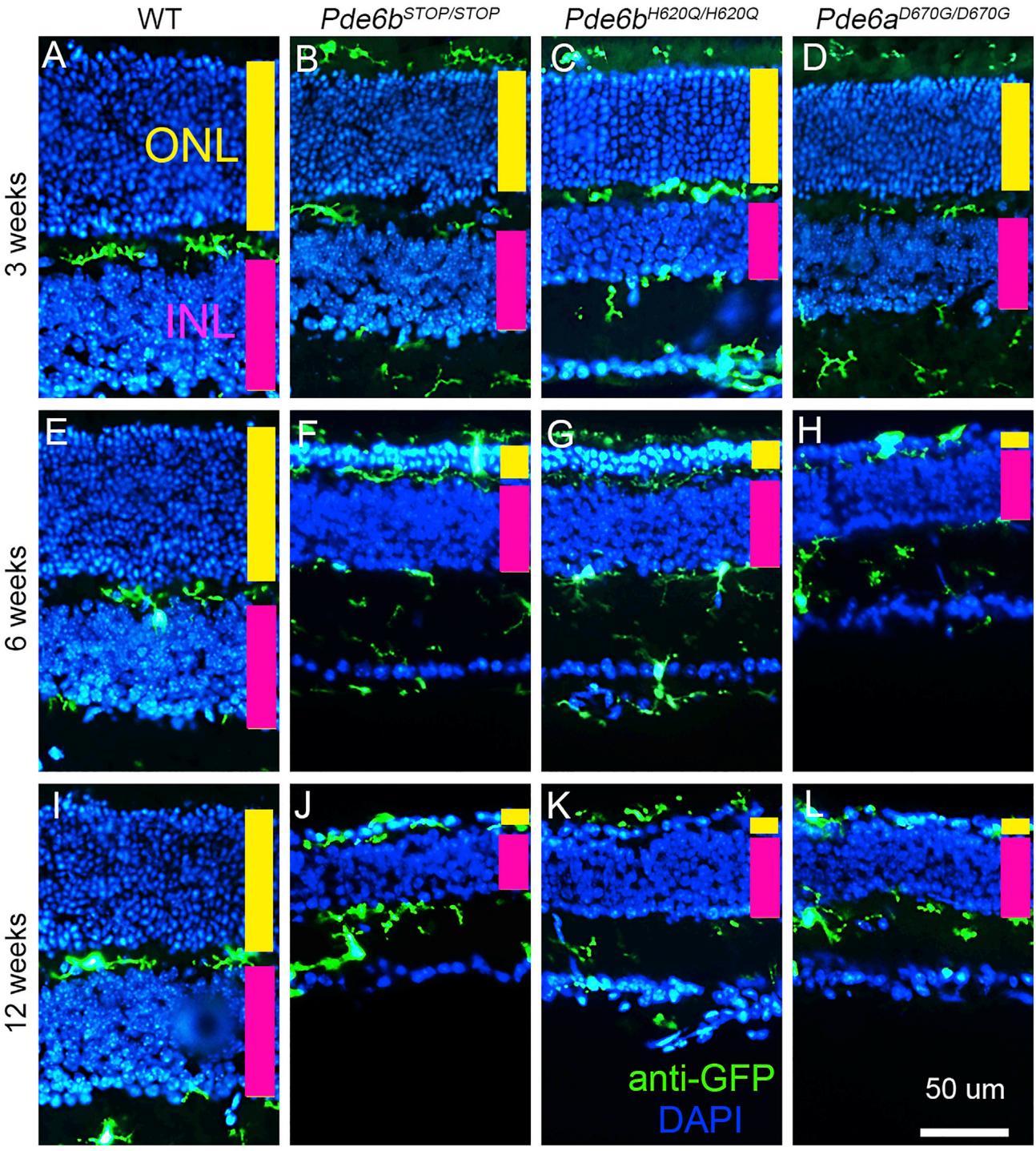

Figure 2. MGCs Migrate to the Layers of the Retina Where Degeneration Is Occurring

Vertical retinal sections were collected from *Pde6b*$^{H620Q/H620Q}$, *Pde6b*$^{STOP/STOP}$, *Pde6a*$^{D670G/D670G}$, and WT mice at 3 (A–D), 6 (E–H), and 12 weeks (I–L). Nuclei were stained with DAPI (blue). Immunostaining with anti-GFP (green) is targeted to MGCs. All sections were crossed by the optic nerve and collected from the medial area of the retina (scale bar, 50 μm; yellow bar, ONL; magenta bar, INL layer).

were seen to localize to the outer and inner plexiform and ganglion cell layers (Figures 2A, 2E, and 2I). In the degeneration models, however, the MGCs, which appeared to be activated given their enlarged, balloon-like shapes and short, broad processes, migrated from the inner retina to the outer retina[34] and phagocytosed photoreceptor debris.[12] Activated MGCs were also found from the ganglion cell layer to the inner plexiform layer as well as from the outer plexiform layer to the inner segment/outer segment (IS/OS) layer at all time points in each mutant model. Roughly only one ONL was observed as early as 6 weeks in the *Pde6a*$^{D670G/D670G}$ mouse model (Figure 2H), whereas this occurred at 12 weeks for the other two RP models (Figures 2J, 2K, and 2L).

Cre-Conditional *Pde6b*$^{H620Q/STOP}$;*Pde6g*$^{Cre/+}$;*Cx3cr1-GFP*$^{+/-}$ Mice Exhibit Increased MGC Density in Conjunction with Increasing Photoreceptor Degeneration

The mouse model *Pde6b*$^{H620Q/STOP}$;*Pde6g*$^{Cre/+}$;*Cx3cr1-GFP*$^{+/-}$ (hereon referred to as *Pde6b*$^{H620Q/STOP}$*Pde6g*$^{Cre/+}$) was created. Activation of Cre leads to the removal of the STOP cassette, allowing the expression of functional PDE6 as previously described.[24] Prior to tamoxifen administration, we characterized the phenotypic manifestations of this mouse model (Figure 3), which experienced retinal degeneration due to an H620Q missense mutation in one allele of the *Pde6b* gene and a Cre-reversible STOP cassette in the other.

OCT imaging, as described previously, was obtained to observe both RP progression in this mouse model at multiple time points compared to the 4-week wild type (WT) (*Pde6b*$^{H620Q/+}$; *Pde6g*$^{Cre/+}$;*Cx3cr1-GFP*$^{+/-}$) (Figures 3A and 3C) as well as MGC localization labeled with *Cx3cr1*::GFP (Figure 3E). The thickness of the ONL decreased with time, with the thinnest length observed at 16 weeks. Live SLO images (Figures 3B and 3D) and retinal flat mount immunoreactivity of *Cx3cr1*::GFP (Figure 3F) displayed a statistically significant difference in MGC density at each time point compared to WT. The MGC density was stable from week 6 to 12.

These results confirmed that the *Pde6b*$^{H620Q/STOP}$*Pde6g*$^{Cre/+}$ mouse phenotype and MGC activation were similar to that observed in the *Pde6b*$^{H620Q/H620Q}$, *Pde6b*$^{STOP/STOP}$, and *Pde6a*$^{D670G/D670G}$ mouse models, which were shown previously. The level of degeneration in the *Pde6b*$^{H620Q/STOP}$*Pde6g*$^{Cre/+}$ mice, however, appeared to be milder than that of the other three models, as even at 16 weeks, there were still roughly two rows of photoreceptors in the ONL remaining compared to only one row remaining in the other three models. Additionally, GFP was observed in the ONL and IS/OS layers along with a higher density of MGCs. These MGCs were shorter and broader compared to those in WT at all time points. These findings were comparable with the observations acquired from the *Pde6b*$^{H620Q/H620Q}$, *Pde6b*$^{STOP/STOP}$, and *Pde6a*$^{D670G/D670G}$ mouse models.

Genetic Rescue Stops the Progression of Photoreceptor Degeneration and Reverses the Activity of MGCs

Tamoxifen was injected intraperitoneally into the *Pde6b*$^{H620Q/STOP}$; *Pde6g*$^{Cre/+}$ mice, resulting in the translocation of the Cre recombinase and removal of the STOP cassette. This allows the *Pde6*^{STOP} allele to be corrected to *Pde6*$^{+}$, which expresses the normal functional PDE6 protein and helps halt the progression of degeneration.

The *Pde6b*$^{H620Q/STOP}$;*Pde6g*$^{Cre/+}$ mice were divided into three groups based on when tamoxifen treatment was administered: 2, 4, or 8 weeks postnatally. Live OCT and SLO images were obtained at 2, 6, and 14 weeks after tamoxifen treatment. These images were measured and quantified (Figure 4). No significant difference in photoreceptor thickness was detected from week 2 onward in the mice treated at 2 weeks compared to WT (*Pde6b*$^{H620Q/+}$; *Pde6g*$^{Cre/+}$;*Cx3cr1-GFP*$^{+/-}$) (Figure 4B). When the mice were treated at 4 and 8 weeks, the difference in photoreceptor thickness was always significant compared to WT, but as seen in the 2-week treatment group, the thicknesses remained at relatively constant levels at each imaging time point (Figures 4E and 4H). This suggests that the degeneration of photoreceptors halted within the first 2 weeks after tamoxifen injection regardless of when treatment occurred (Figure 5A). The MGC density was significantly higher in the mutant mice at 2 weeks after treatment compared to WT (Figures 4C, 4F, and 4I). At 6 and 14 weeks after treatment, however, the MGC density reached levels similar to those of WT for all treatment groups, suggesting that the density decreased between 2 and 6 weeks after treatment (Figure 5B).

Fate mapping of MGCs in retinal cross-sections of *Pde6b*$^{H620Q/STOP}$; *Pde6g*$^{Cre/+}$ mice at 2, 6, and 14 weeks after treatment (Figure 6) was performed by assessing the location of CX3CR1::GFP immunoreactivity. The degeneration of photoreceptors was halted 2 weeks after treatment. The GFP signal, which is co-expressed with the MGC-specific marker CX3CR1, was identified in the ganglion cell layer, inner plexiform layer, and outer plexiform layer. No GFP was identified in the ONL or in the IS/OS layer, where the photoreceptor degeneration halted within 2 weeks after treatment. Loss of the CX3CR1 marker revealed deactivation of MGCs following restoration of *Pde6b* expression in the *Pde6b*$^{H620Q/STOP}$;*Pde6g*$^{Cre/+}$ mouse model.

MGCs Are Deactivated as a Result of Genetic Rescue

Whole-mount anti-GFP immunohistochemistry images acquired from retinal flat mounts harvested before and after tamoxifen treatment in the *Pde6b*$^{H620Q/STOP}$;*Pde6g*$^{Cre/+}$ mice were compared against normal WT to confirm that the deactivation of MGCs was a result of genetic rescue (Figure 7). The MGCs before treatment were imaged 2 weeks postnatally. Tamoxifen was injected that same day to begin monitoring the MGC phenotype over the course of 1, 2, 3, and 4 weeks after treatment. At 1 week after treatment, the MGCs remained activated, exhibiting balloon-like morphology that is similar to that of the MGCs before tamoxifen treatment. From 2 weeks after treatment and onward, however, fewer dendritic branches and decreased balloon-like morphology were observed, resulting in a phenotype that closely resembles that of the normal WT retina. This suggests that the MGCs were deactivated after genetic rescue was performed.

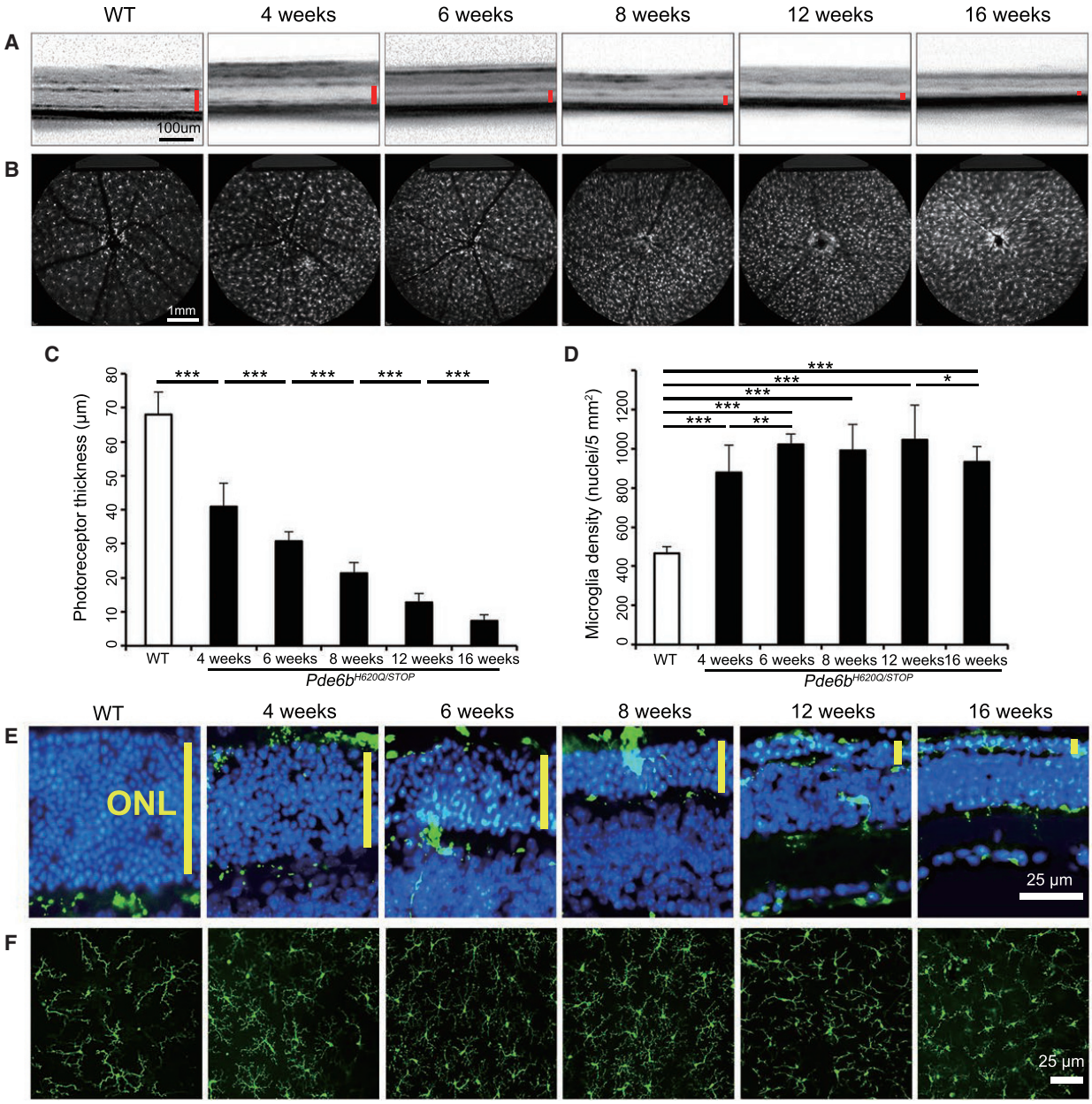

Figure 3. MGC Density Increases in Conjunction with Increased Photoreceptor Degeneration

(A and B) Live OCT (A) and SLO (B) images were taken from the *Pde6b*$^{H620Q/STOP}$;*Pde6g*$^{Cre/+}$ mouse model at 4, 6, 8, 12, and 16 weeks, while the WT was imaged at 4 weeks (red bar, ONL and IS/OS; for OCT, scale bar, 100 μm; for SLO, scale bar, 1 mm). (C and D) Photoreceptor thickness and MGC density were measured and quantified using the techniques outlined in Figure 1. (C) $p < 0.001$ for WT compared to each mutant mouse and between each mutant mouse. (D) $p < 0.001$ for WT compared to mutant mice at all time points. No statistically significant difference was found between 6, 8, and 12 weeks in the mutant mouse. $p = 0.002$ between 4 and 6 weeks. (E and F) Retinal cross sections (E) and retinal flat mounts (F) were stained at 4, 6, 8, 12, and 16 weeks for the mutant mice compared to at 4 weeks for WT (blue, DAPI; green, GFP; yellow bar, ONL; scale bar, 25 μm). *$p < 0.05$; **$p < 0.01$; ***$p < 0.001$. Error bars are 1 SD.

DISCUSSION

MGCs are widely studied in the CNS and retina, as they perform key roles in both physiological and pathological processes. These roles include modulation of the inflammatory and immune response,[35] phagocytosis,[2,36] antigen presentation, recognition of pathogens and bound antibodies, and cytotoxicity.[37,38] In the retina, the main function of MGCs is phagocytosis, which involves clearing tissue debris,[2] aberrant neurons, and synapses.[37] In addition, MGCs can exist as

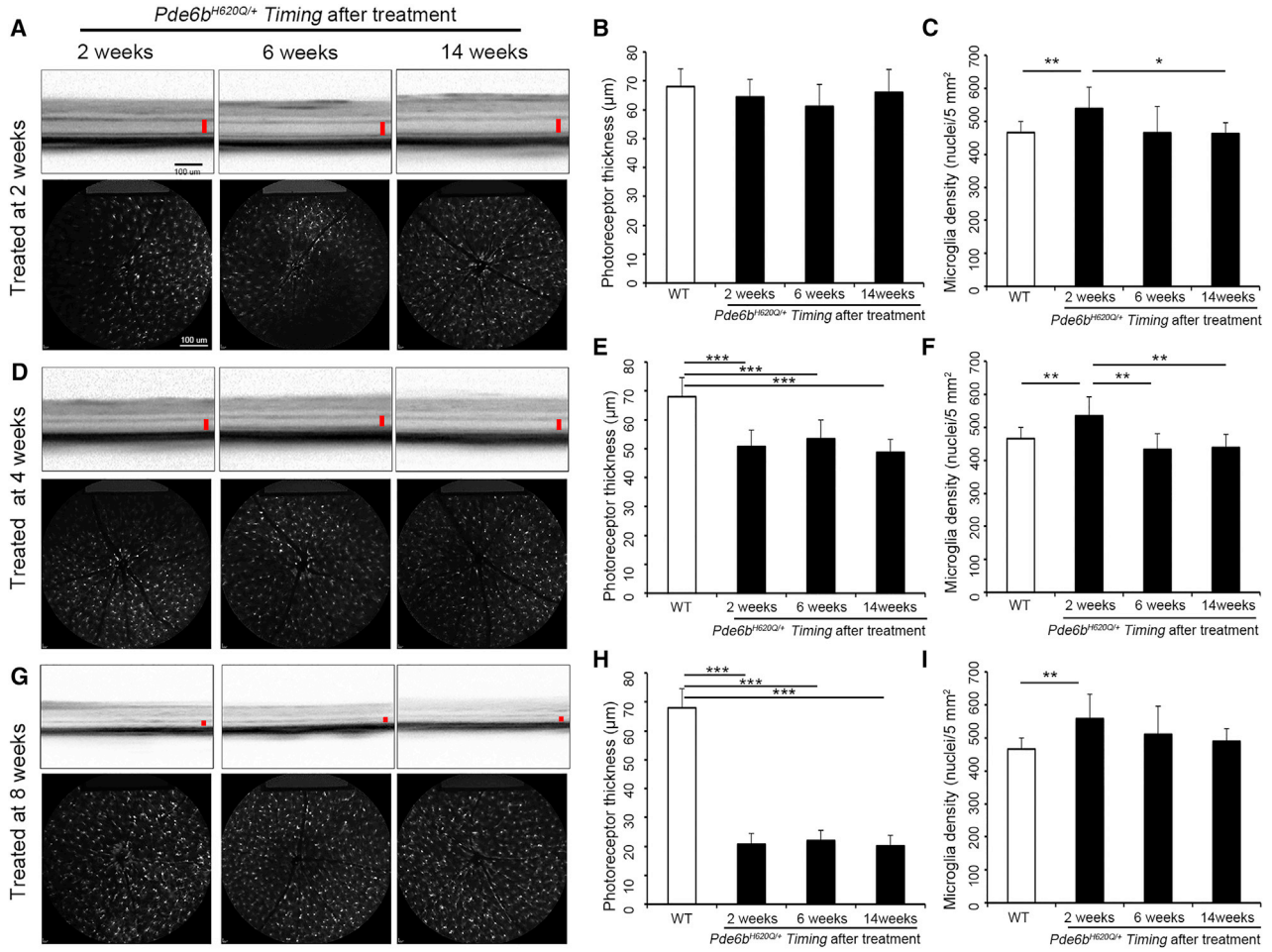

Figure 4. Genetic Rescue Arrested the Increase in MGC Density in *Pde6b*$^{H620Q/STOP}$*Pde6g*$^{Cre/+}$ Mouse Models

Pde6b$^{H620Q/STOP}$;*Pde6g*$^{Cre/+}$ mice were treated with intraperitoneal tamoxifen injections at 2, 4, and 8 weeks postnatally. (A, D, and G) Live OCT (top) and SLO (bottom) images were acquired at 2, 6, and 14 weeks after treatment, as described previously (OCT scale bar, 100 μm; red bar, ONL and IS/OS layers; SLO scale bar, 1 mm). (B, E, and H) Photoreceptor thickness in mice treated at 2, 4, and 8 weeks was measured and quantified based on the OCT images at each time point compared to WT. (B) No statistical difference was detected between mutant groups or compared to WT. (E and H) Compared to WT and mutant mice at all time points, $p < 0.001$. No statistical difference was detected at any time point between mutant groups. (C, F, and I) MGC density in mice treated at 2, 4, and 8 weeks was measured and quantified based on the SLO images at each time point compared to WT. (C) $p = 0.008$ for WT compared to mutant mice 2 weeks after treatment. No difference was found when WT was compared at 6 and 14 weeks. (F) $p = 0.007$ for WT compared to mutant mice 2 weeks after treatment. No difference was found when WT was compared at 6 and 14 weeks. (I) $p = 0.003$ for WT compared to mutant mice 2 weeks after treatment. No difference found when WT was compared at 6 and 14 weeks. *$p < 0.05$; **$p < 0.01$; ***$p < 0.001$. Error bars are 1 SD.

other morphological states such as rod MGCs and multinucleated MGCs.[37] After birth, the renewal of the MGC pool primarily relies on the self-proliferation of embryonic invaded MGCs, namely the resident MGCs.[39,40] One of the most commonly used mouse models in MGC research is the CX3CR::EGFP mouse line, in which all MGCs are GFP positive. The CX3CL1-CX3CR1 axis is one of the most prominent ligand-receptor pairs that are specifically expressed in MGCs for a variety of inhibitory factors that are constitutively expressed in the retina and brain.[3,41,42]

We characterized the effects of neurodegeneration on MGC activation in the retina via the CX3CR1 receptor in living mice with retinal degeneration due to PDE6 deficiency. In this study, we crossed several mouse lines to obtain the *Pde6a*$^{D670G/D670G}$;*Cx3cr1-GFP*$^{+/-}$, *Pde6b*$^{H620Q/H620Q}$;*Cx3cr1-GFP*$^{+/-}$, *Pde6b*$^{STOP/STOP}$;*Cx3cr1-GFP*$^{+/-}$, *Pde6b*$^{H620Q/STOP}$;*Cx3cr1-GFP*$^{+/-}$, and WT;*Cx3cr1-GFP*$^{+/-}$ mouse models. These models exhibit GFP expression under the control of *Cx3cr1*, which specifically marks MGCs in the retina.[43–45] GFP expression can be detected using immunocytochemistry after the mice are sacrificed and also by quantifying expression after images are obtained from SLO in the living mice. Here, we used live OCT and immunolocation and SLO imaging to characterize the density, distribution, and morphology of MGCs. The combination of SLO and immunostaining of GFP shows that MGCs are activated in

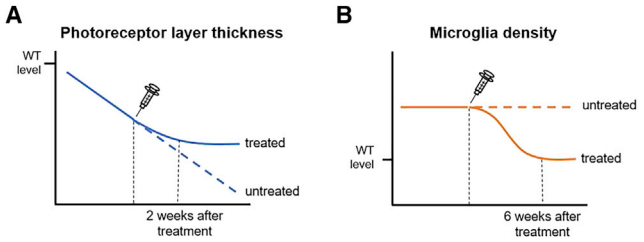

Figure 5. A Schematic Illustration Summarizing the Effects of Tamoxifen Treatment on MGCs and Photoreceptors in *Pde6b*$^{H620Q/STOP}$*Pde6g*$^{Cre/+}$ Mouse Models

(A) A line graph comparing the photoreceptor layer thickness between treated (solid blue line) and untreated (dotted blue line) *Pde6b*$^{H620Q/STOP}$*Pde6g*$^{Cre/+}$ mice over time. Approximately 2 weeks after treatment, the photoreceptor layer thickness in *Pde6b*$^{H620Q/STOP}$*Pde6g*$^{Cre/+}$ mice plateaus and remains constant over time. (B) A line graph comparing MGC density between treated (solid orange line) and untreated (dotted orange line) *Pde6b*$^{H620Q/STOP}$*Pde6g*$^{Cre/+}$ mice over time. MGC density and inflammation returned to normal WT levels by 6 weeks after tamoxifen treatment.

multiple RP mouse models, migrating to the IS/OS layer and ONL, where the degeneration of photoreceptors occurs. In the *Pde6a*$^{D670G/D670G}$ mouse model, we found that MGCs congregated to form denser areas, which suggested that degeneration is not uniform throughout the retina, leading to patches of atrophy where MGCs are concentrated. No such patches of atrophy as shown in the *Pde6a*$^{D670G/D670G}$ mouse model were found in the other three mutant mouse models, but a decrease in ONL thickness and an increase in MGC density were found in all four mutant mouse models. These results further confirm that MGCs are activated and contribute to the progression of photoreceptor degeneration in RP with multiple genetic backgrounds. Based on continuous observation of the *Pde6b*$^{H620Q/STOP}$ mouse model, retinal degeneration progresses over time until the late-onset stage, in which all the photoreceptor cells, including cones, die. The density of MGCs increases in the mutant mice and reaches a plateau during the middle stage of disease progression before the degeneration is completed.

In the current study, we established a *Pde6b*$^{H620Q/STOP}$;*Pde6g*$^{Cre/+}$;*Cx3cr1-GFP*$^{+/--}$ mouse model with a STOP cassette in one of the diseased *Pde6b* alleles that can be reversed when Cre is activated by intraperitoneal tamoxifen injection.[23–25] The *Pde6b*$^{H620Q/STOP}$;*Pde6g*$^{Cre/+}$;*Cx3cr1-GFP*$^{+/-}$ mouse model, however, exhibits a slower progression than *Pde6a*$^{D670G/D670G}$ and *Pde6b*$^{STOP/STOP}$, which provides a longer therapeutic window for distinguishing the characteristic of MGCs. Gene replacement therapy could potentially lead to a treatment in which disease progression is halted through the restoration of continuous, normal protein expression via gene therapy, similar to what occurs in our Cre-inducible rescue model. In this study, we observed increased MGC density and activated MGC morphology during the progression of photoreceptor degeneration in all of the mutant mice. Moreover, we found that the degeneration of photoreceptors was halted within 2 weeks after gene replacement therapy was applied, and at week 6 after treatment, the activated MGCs in the degeneration site disappeared, as MGCs with inactivated morphology were found only in the ganglion cell layer, inner plexiform layer, and outer plexiform layer. Surprisingly, we found that the morphology and density of activated MGCs during photoreceptor degeneration could return to a normal level after treatment. Hence, whether the MGCs are activated or not could be used as a marker to test if the treatment for RP is effective. Moreover, we hypothesize that effective genetic rescue methods that aim to target and decrease MGC activation may serve as potential therapies for RP, given that there may be a causal relationship between activated MGCs and increased photoreceptor degeneration in the retina. However, more studies are needed to investigate this hypothesis.

In designing how to rescue the preclinical models from RP progression, we considered two different genetic rescue approaches: viral-based gene replacement therapy and intraperitoneal tamoxifen Cre-loxP gene switch. Though gene therapy may be established after onset of disease, as in slower degenerating mouse models, the Cre-loxP system is more stable, practical, and easily repeatable for the purposes of our project. First, the interphotoreceptor matrix, which reaches maturity around postnatal day 15, blocks viral contact with the photoreceptor plasma membrane.[46,47] Second, subretinal injection of virus induces trauma, which complicates post-injury MGC morphogenesis, retinal rewiring,[48] and data interpretation. Third, an important limitation of viral-based gene therapy is the large variance in rescue, partly due to the difficulty in successfully quantifying subretinal transduction. Finally, after postnatal day 5, mice cannot be cryoanesthetized, which is a standard Institutional Animal Care and Use Committee-approved procedure for subretinal viral gene therapy.[49,50] All of these challenges were avoided in this study by using our inducible Cre-loxP method, which affords the temporal control required for gene delivery at any time point while also allowing for control of the target cell(s).

As discussed above, MGCs play an important role in cell protection against pathogens and other insults, but can also contribute to disease progression and cause harm by promoting neuroinflammation, which is cytotoxic and serves to induce death in neighboring cells.[9–12] Our data agree with findings acquired in similar studies of MGC activation. In a study of retinal degenerative conditions, Gupta et al.[12] found that the MGCs were enlarged compared to controls and stained positively for markers of rod photoreceptors. The researchers also found that retinal MGCs in patients with these conditions were activated more quickly by rod cell death, and they hypothesized that activated MGCs release cytotoxic factors that may contribute to the gradual death of cones. Similar findings have been observed in studies of glaucoma and age-related macular degeneration as well.[51,52] Similarly, in a mouse model of RP,[53] minocycline was used to inhibit MGC activation, and a chemokine receptor, CX3CR1, was identified as playing a potential role in the disease progression. Specifically, transgenic *rd10/Cx3cr1*$^{GFP/GFP}$ mice had significantly decreased functionality as measured by electroretinogram (ERG). Another study of Cx3cr1 in a paraquat-induced model of retinal degeneration showed that Cx3cr1 deficiency leads to increased inflammation.[54]

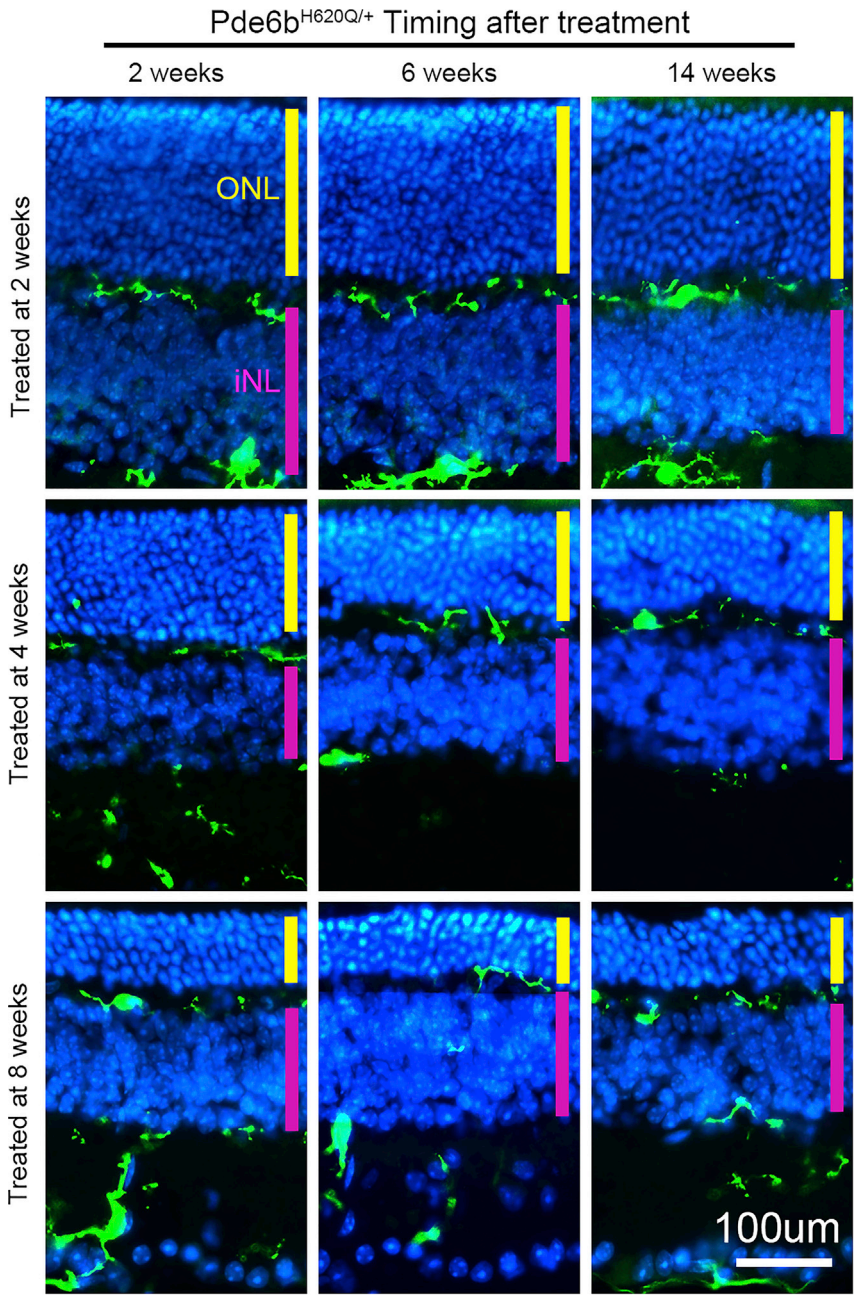

Figure 6. Genetic Rescue Reversed the Migration of Microglia

Microglial CX3CR1 expression was studied in *Pde6b*$^{H620Q/STOP}$;*Pde6g*$^{Cre/+}$ retinal cross-sections at 2, 6, and 14 weeks after treatment. No CX3CR1 signal was detected in the IS/OS layer and ONL. The thickness of the ONL and photoreceptor nuclear density remained at the same level from 2 to 14 weeks for all three different time points of treatment (green, GFP; blue, DAPI; yellow bar, ONL; magenta bar, INL; scale bar, 100 μm).

In this unique study, we showed that genetic rescue can be used to halt RP disease progression and study MGC density at different time points. Together, our data suggested that MGCs play an important role in RP and that genetic rescue helps reduce their density and mislocalization, regardless of the time of treatment intervention. Furthermore, although many gene therapy interventions are promising, they often fail to halt disease progression long-term. Long-term halting of disease progression might be made more efficacious by downregulating MGC activity while co-administering the therapeutic intervention. MGCs in the context of retinal immune responses in gene therapy are an important yet neglected field of study that merits further work, as it holds the potential to strengthen available therapies.

MATERIALS AND METHODS

The Institutional Animal Care and Use Committee (IACUC) at Columbia University approved all experiments prior to experimentation.

Animals

Mice were used in accordance with the statement for the use of animals in ophthalmic and vision research of the Association for Research in Vision and Ophthalmology, as well as the policy on the Use of Human Subjects in Neuroscience Research of the Society for Neuroscience. *Cx3cr1::GFP* mice (stock #005582) were obtained from The Jackson Laboratory (Harbor, ME, USA). *Pde6b*^{STOP} mice and *Pde6g* ^{CreERT2} mice were generated at Jonas Children's Vision Care, as previously described.[24,25] *Pde6b*^{H620Q} mice were rederived via oviduct transfer from morulae which were provided by the European Mouse Mutant Archive (EMMA).[55,56] *Pde6a*^{D670G} mice (C57BL/6J-*Pde6a*$^{nmf363/nmf363}$) were obtained from Jackson Laboratory (Bar Harbor, ME, USA). All mice were maintained in the Columbia University Pathogen-free Eye Institute Annex Animal Care Services Facility under a 12/12-hr light/dark cycle, with food and water available *ad libitum*. Efforts were made to minimize animal suffering and numbers. All mice, including WT, were crossed with *Cx3cr1::GFP* mice in order to visualize MGCs in the retina.

The cSLO Imaging

0.1 mL/10 g body weight (BW) of anesthetic solution (1 mL of 100 mg/mL ketamine, 0.1 mL of 20 mg/mL xylazine, and 8.9 mL of PBS) was used to anesthetize mice via intraperitoneal injection. Dilation was achieved with a combination of 2.5% phenylephrine hydrochloride (Paragon) and 1% tropicamide (Akorn) administered topically. A heating pad was used to maintain body temperature at

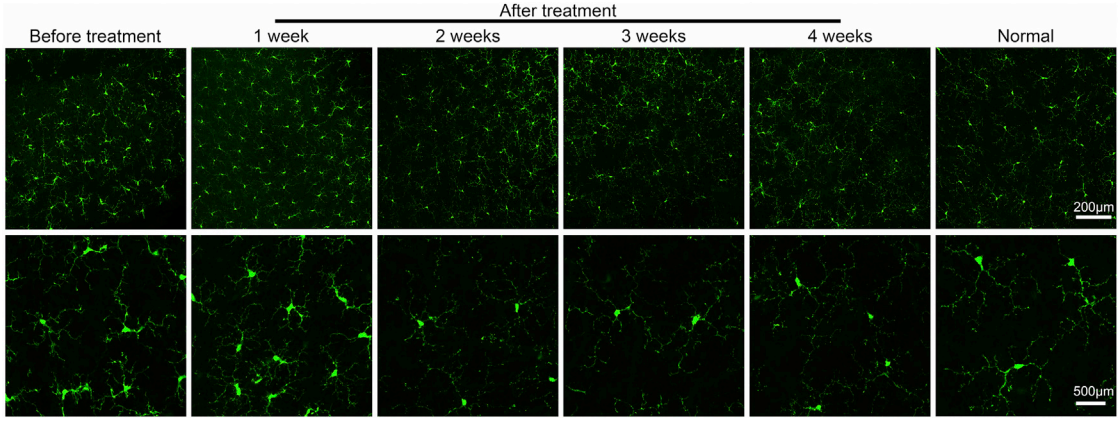

Figure 7. MGCs Were Deactivated After Genetic Rescue Was Performed

Retinal flat mounts were harvested from treated and untreated *Pde6b*$^{H620Q/STOP}$;*Pde6g*$^{Cre/+}$;*Cx3cr1-GFP*$^{+/-}$ mice as well as from WT *Pde6b*$^{H620Q/+}$;*Pde6g*$^{Cre/+}$;*Cx3cr1-GFP*$^{+/-}$ mice. Images in the bottom row are magnified images of a portion of MGCs seen in the top row. The MGCs of the before-treatment group were imaged at postnatal day 14. The mice in the treatment group were given tamoxifen on postnatal day 14 and imaged weekly for 4 weeks (green, anti-GFP; top row scale bar, 200 μm; bottom row scale bar, 500 μm).

37°C. Until the pupil was fully diluted, Gonioscopic Prism solution (Akorn) was applied to both eyes to prevent dry eyes. The tested eye was washed with Balanced salt water (Alcon Laboratories, Fort Worth, Texas). A custom-made platform was used to position anesthetized mice on the forehead rest of a cSLO (Spectralis HRA; Heidelberg Engineering, Heidelberg, Germany). Tested eyes were administered with hydroxypropyl methylcellulose (Akorn) to maintain corneal moisture during the imaging session. The infrared mode of the Spectralis was utilized to locate and focus on the large retinal vessels of the fundus to enable consistent imaging of retinal layers in all mice. Centered on the optic nerve, SLO images were acquired at a resolution of 768 × 768 pixels using the 55° wide-field lens mounted on a Heidelberg Spectralis device. The superficial vascular plexus was used as a point of focus for each image for consistency. The laser power was set at approximately 280 μW with a sensitivity of 100. Because the true-track mode was not available at the time of image acquisition, images were manually aligned with previously recorded images in the same imaging session. Images were analyzed by ImageJ (https://imagej.nih.gov/ij/; provided in the public domain by the NIH, Bethesda, MD, USA).

OCT

OCT imaging was performed directly following SLO imaging so that animals remained anesthetized. The commercially available HRA + OCT device (Spectralis; Heidelberg Engineering, Heidelberg, Germany) equipped with a broadband super-luminescent diode at λ = 880 nm as a low coherent light source was used. Two-dimensional B-scan recordings were acquired with a 30° lens, and each scan consisted of 768 A-scans acquired at a speed of 40,000 scans per second. Images were also analyzed by ImageJ.

Tamoxifen Injection

Tamoxifen (100 mg/mL in ethanol; Sigma-Aldrich T5648) was mixed thoroughly at 42°C, then diluted to a final concentration of 2 mg/mL with corn oil. The solution was then injected intraperitoneally once per day for 3 consecutive days at a concentration of 100 μg/g BW, beginning at the time points described in the Results section.

Immunohistochemistry

Mice were euthanized following established IACUC guidelines. Eyes were enucleated, with the upward cornea labeled to ensure all retinas were cut in the same fashion. Subsequently, eyes were placed in 4% paraformaldehyde for 5 min, and then the anterior segment (including the cornea, lens, and vitreous) was removed. The posterior segment was then placed into another 4% paraformaldehyde bath for 45 min, washed three times with PBS for 5 min, then cryoprotected in 30% sucrose overnight. The posterior eye cup was then embedded in optimal cutting temperature compound (Thermo Fisher Scientific, Waltham MA) and sectioned from temporal to nasal at 8 μm using a cryostat (Leica). All sections were post-fixed with 4% paraformaldehyde for 20 min, then washed and incubated with PBS containing 0.3% Triton X-100 (PBST) and 5% ChemiBLOCKER (2170, Millipore) at room temperature for 1 hr. Sections were washed again with PBST and incubated overnight at 4°C with primary antibody. The following antibodies were used: Alexa Fluor 488-conjugated anti-GFP (1;1,000; catalog A-21311; Thermo Fisher), Cy3-coupled anti-GFAP (1:800; catalog C9205; Sigma-Aldrich). Sections were subsequently washed again with PBST for 10 min, three times, then incubated in 5 μg/mL Hoechst 33342 (H13999, Molecular Probes, Life Technologies) for 5 min and finally imaged using a confocal microscope (Nikon A1).

Whole-Mount Immunohistochemistry

Retinas were fixed in 4% paraformaldehyde for 20 min, washed, and stained as described above. For each whole-mounted retina, six images were obtained at 10× and 20× magnificent on a Nikon Eclipse Ti microscope and then merged using NIS-elements AR 4.40.00 software.

Statistical Analysis

Statistical analysis was performed by using GraphPad Prism, version 6 (GraphPad Software, CA, USA); *$p < 0.05$ was treated as statistically significant and **$p < 0.01$ and **$p < 0.001$.

AUTHOR CONTRIBUTIONS

S.H.T. and L.Z. designed the experiments; L.Z. and X.C. conducted the experiments; S.H.T. and X.C. composed the manuscript; L.Z. collected the data; X.C., S.J., and J.K.D. analyzed the data; X.C., R.J., and K.S.P. prepared the images and figures; Y.-T.T., C.-W.H., W.-H.W., C.L.X., and C.S.L. provided technical support; S.H.T. and L.Z. obtained funding; S.H.T supervised the study and provided all materials and administrative support.

CONFLICTS OF INTEREST

The authors declare no conflicts of interest.

ACKNOWLEDGMENTS

L.Z. is supported by the National Natural Science Foundation of China (81500750). The Jonas Children's Vision Care and Bernard & Shirlee Brown Glaucoma Laboratory are supported by the NIH (P30EY019007, R01EY018213, R01EY024698, R01EY026682, R21AG050437), National Cancer Institute Core (5P30CA013696), the Research to Prevent Blindness (RPB) Physician-Scientist Award, and unrestricted funds from the RPB, New York, NY, USA. S.H.T. is a member of the RD-CURE Consortium and is supported by the Tistou and Charlotte Kerstan Foundation, the Schneeweiss Stem Cell Fund, New York State (C029572), the Foundation Fighting Blindness (TA-NMT-0116-06-COLU), and the Gebroe Family Foundation. R.J. is supported by the RPB Medical Student Eye Research Fellowship.

REFERENCES

1. Langmann, T. (2007). Microglia activation in retinal degeneration. J. Leukoc. Biol. *81*, 1345–1351.
2. Kettenmann, H., Hanisch, U.K., Noda, M., and Verkhratsky, A. (2011). Physiology of microglia. Physiol. Rev. *91*, 461–553.
3. Ransohoff, R.M., and Perry, V.H. (2009). Microglial physiology: unique stimuli, specialized responses. Annu. Rev. Immunol. *27*, 119–145.
4. Arroba, A.I., and Valverde, A.M. (2017). Modulation of microglia in the retina: new insights into diabetic retinopathy. Acta Diabetol. *54*, 527–533.
5. Nimmerjahn, A., Kirchhoff, F., and Helmchen, F. (2005). Resting microglial cells are highly dynamic surveillants of brain parenchyma in vivo. Science *308*, 1314–1318.
6. Kreutzberg, G.W. (1996). Microglia: a sensor for pathological events in the CNS. Trends Neurosci. *19*, 312–318.
7. Wang, J., Yang, Z., Liu, C., Zhao, Y., and Chen, Y. (2013). Activated microglia provide a neuroprotective role by balancing glial cell-line derived neurotrophic factor and tumor necrosis factor-α secretion after subacute cerebral ischemia. Int. J. Mol. Med. *31*, 172–178.
8. Chen, C.W., Chen, Q.B., Ouyang, Q., Sun, J.H., Liu, F.T., Song, D.W., and Yuan, H.B. (2012). Transient early neurotrophin release and delayed inflammatory cytokine release by microglia in response to PAR-2 stimulation. J. Neuroinflammation *9*, 142.
9. Saijo, K., and Glass, C.K. (2011). Microglial cell origin and phenotypes in health and disease. Nat. Rev. Immunol. *11*, 775–787.
10. Lucin, K.M., and Wyss-Coray, T. (2009). Immune activation in brain aging and neurodegeneration: too much or too little? Neuron *64*, 110–122.
11. Cai, Z., Hussain, M.D., and Yan, L.J. (2014). Microglia, neuroinflammation, and beta-amyloid protein in Alzheimer's disease. Int. J. Neurosci. *124*, 307–321.
12. Gupta, N., Brown, K.E., and Milam, A.H. (2003). Activated microglia in human retinitis pigmentosa, late-onset retinal degeneration, and age-related macular degeneration. Exp. Eye Res. *76*, 463–471.
13. Daiger, S.P., Bowne, S.J., and Sullivan, L.S. (2014). Genes and Mutations Causing Autosomal Dominant Retinitis Pigmentosa. Cold Spring Harb. Perspect. Med. *5*, a017129.
14. Sengillo, J.D., Justus, S., Tsai, Y.T., Cabral, T., and Tsang, S.H. (2016). Gene and cell-based therapies for inherited retinal disorders: An update. Am. J. Med. Genet. C. Semin. Med. Genet. *172*, 349–366.
15. Hamel, C. (2006). Retinitis pigmentosa. Orphanet J. Rare Dis. *1*, 40.
16. Wambach, J.A., Casey, A.M., Fishman, M.P., Wegner, D.J., Wert, S.E., Cole, F.S., Hamvas, A., and Nogee, L.M. (2014). Genotype-phenotype correlations for infants and children with ABCA3 deficiency. Am. J. Respir. Crit. Care Med. *189*, 1538–1543.
17. Narayan, D.S., Wood, J.P., Chidlow, G., and Casson, R.J. (2016). A review of the mechanisms of cone degeneration in retinitis pigmentosa. Acta Ophthalmol. *94*, 748–754.
18. McLaughlin, M.E., Ehrhart, T.L., Berson, E.L., and Dryja, T.P. (1995). Mutation spectrum of the gene encoding the beta subunit of rod phosphodiesterase among patients with autosomal recessive retinitis pigmentosa. Proc. Natl. Acad. Sci. USA *92*, 3249–3253.
19. Dryja, T.P., Rucinski, D.E., Chen, S.H., and Berson, E.L. (1999). Frequency of mutations in the gene encoding the alpha subunit of rod cGMP-phosphodiesterase in autosomal recessive retinitis pigmentosa. Invest. Ophthalmol. Vis. Sci. *40*, 1859–1865.
20. Wensel, T.G., Zhang, Z., Anastassov, I.A., Gilliam, J.C., He, F., Schmid, M.F., and Robichaux, M.A. (2016). Structural and molecular bases of rod photoreceptor morphogenesis and disease. Prog. Retin. Eye Res. *55*, 32–51.
21. Farber, D.B. (1995). From mice to men: the cyclic GMP phosphodiesterase gene in vision and disease. The Proctor Lecture. Invest. Ophthalmol. Vis. Sci. *36*, 263–275.
22. Tsang, S.H., Chan, L., Tsai, Y.T., Wu, W.H., Hsu, C.W., Yang, J., Tosi, J., Wert, K.J., Davis, R.J., and Mahajan, V.B. (2014). Silencing of tuberin enhances photoreceptor survival and function in a preclinical model of retinitis pigmentosa (an american ophthalmological society thesis). Trans. Am. Ophthalmol. Soc. *112*, 103–115.
23. Koch, S.F., Duong, J.K., Hsu, C.W., Tsai, Y.T., Lin, C.S., Wahl-Schott, C.A., and Tsang, S.H. (2017). Genetic rescue models refute nonautonomous rod cell death in retinitis pigmentosa. Proc. Natl. Acad. Sci. USA *114*, 5259–5264.
24. Koch, S.F., Tsai, Y.T., Duong, J.K., Wu, W.H., Hsu, C.W., Wu, W.P., Bonet-Ponce, L., Lin, C.S., and Tsang, S.H. (2015). Halting progressive neurodegeneration in advanced retinitis pigmentosa. J. Clin. Invest. *125*, 3704–3713.
25. Davis, R.J., Hsu, C.W., Tsai, Y.T., Wert, K.J., Sancho-Pelluz, J., Lin, C.S., and Tsang, S.H. (2013). Therapeutic margins in a novel preclinical model of retinitis pigmentosa. J. Neurosci. *33*, 13475–13483.
26. Chen, P., Zhao, W., Guo, Y., Xu, J., and Yin, M. (2016). CX3CL1/CX3CR1 in Alzheimer's Disease: A Target for Neuroprotection. BioMed Res. Int. *2016*, 8090918.
27. Feng, X., Szulzewsky, F., Yerevanian, A., Chen, Z., Heinzmann, D., Rasmussen, R.D., Alvarez-Garcia, V., Kim, Y., Wang, B., Tamagno, I., et al. (2015). Loss of CX3CR1 increases accumulation of inflammatory monocytes and promotes gliomagenesis. Oncotarget *6*, 15077–15094.
28. Tristão, F.S., Lazzarini, M., Martin, S., Amar, M., Stühmer, W., Kirchhoff, F., Gomes, L.A., Lanfumey, L., Prediger, R.D., Sepulveda, J.E., et al. (2016). CX3CR1 Disruption Differentially Influences Dopaminergic Neuron Degeneration in Parkinsonian Mice Depending on the Neurotoxin and Route of Administration. Neurotox. Res. *29*, 364–380.
29. Poniatowski, L.A., Wojdasiewicz, P., Krawczyk, M., Szukiewicz, D., Gasik, R., Kubaszewski, Ł., and Kurkowska-Jastrzębska, I. (2017). Analysis of the Role of CX3CL1 (Fractalkine) and Its Receptor CX3CR1 in Traumatic Brain and Spinal Cord Injury: Insight into Recent Advances in Actions of Neurochemokine Agents. Mol. Neurobiol. *54*, 2167–2188.
30. Sutti, S., Heymann, F., Bruzzi, S., Peusquens, J., Trautwein, C., Albano, E., and Tacke, F. (2017). CX3CR1 modulates the anti-inflammatory activity of hepatic dendritic

cells in response to acute liver injury. Clin. Sci. (Lond.). , Published online July 24 2017. https://doi.org/10.1042/CS20171025.

31. Man, A.L., Gicheva, N., Regoli, M., Rowley, G., De Cunto, G., Wellner, N., Bassity, E., Gulisano, M., Bertelli, E., and Nicoletti, C. (2017). CX3CR1+ Cell-Mediated Salmonella Exclusion Protects the Intestinal Mucosa during the Initial Stage of Infection. J. Immunol. *198*, 335–343.

32. Zhao, W., Lu, H., Wang, X., Ransohoff, R.M., and Zhou, L. (2016). CX3CR1 deficiency delays acute skeletal muscle injury repair by impairing macrophage functions. FASEB J. *30*, 380–393.

33. Luna, G., Keeley, P.W., Reese, B.E., Linberg, K.A., Lewis, G.P., and Fisher, S.K. (2016). Astrocyte structural reactivity and plasticity in models of retinal detachment. Exp. Eye Res. *150*, 4–21.

34. Zeng, H., Ding, M., Chen, X.X., and Lu, Q. (2014). Microglial NADPH oxidase activation mediates rod cell death in the retinal degeneration in rd mice. Neuroscience *275*, 54–61.

35. Lampron, A., Elali, A., and Rivest, S. (2013). Innate immunity in the CNS: redefining the relationship between the CNS and Its environment. Neuron *78*, 214–232.

36. Fu, R., Shen, Q., Xu, P., Luo, J.J., and Tang, Y. (2014). Phagocytosis of microglia in the central nervous system diseases. Mol. Neurobiol. *49*, 1422–1434.

37. Boche, D., Perry, V.H., and Nicoll, J.A. (2013). Review: activation patterns of microglia and their identification in the human brain. Neuropathol. Appl. Neurobiol. *39*, 3–18.

38. Kaur, C., Rathnasamy, G., and Ling, E.A. (2013). Roles of activated microglia in hypoxia induced neuroinflammation in the developing brain and the retina. J. Neuroimmune Pharmacol. *8*, 66–78.

39. Bruttger, J., Karram, K., Wörtge, S., Regen, T., Marini, F., Hoppmann, N., Klein, M., Blank, T., Yona, S., Wolf, Y., et al. (2015). Genetic Cell Ablation Reveals Clusters of Local Self-Renewing Microglia in the Mammalian Central Nervous System. Immunity *43*, 92–106.

40. Ajami, B., Bennett, J.L., Krieger, C., Tetzlaff, W., and Rossi, F.M. (2007). Local self-renewal can sustain CNS microglia maintenance and function throughout adult life. Nat. Neurosci. *10*, 1538–1543.

41. Jung, S., Aliberti, J., Graemmel, P., Sunshine, M.J., Kreutzberg, G.W., Sher, A., and Littman, D.R. (2000). Analysis of fractalkine receptor CX(3)CR1 function by targeted deletion and green fluorescent protein reporter gene insertion. Mol. Cell. Biol. *20*, 4106–4114.

42. Biber, K., Neumann, H., Inoue, K., and Boddeke, H.W. (2007). Neuronal 'On' and 'Off' signals control microglia. Trends Neurosci. *30*, 596–602.

43. Kohno, H., Koso, H., Okano, K., Sundermeier, T.R., Saito, S., Watanabe, S., Tsuneoka, H., and Sakai, T. (2015). Expression pattern of Ccr2 and Cx3cr1 in inherited retinal degeneration. J. Neuroinflammation *12*, 188.

44. Zabel, M.K., Zhao, L., Zhang, Y., Gonzalez, S.R., Ma, W., Wang, X., Fariss, R.N., and Wong, W.T. (2016). Microglial phagocytosis and activation underlying photoreceptor degeneration is regulated by CX3CL1-CX3CR1 signaling in a mouse model of retinitis pigmentosa. Glia *64*, 1479–1491.

45. Beli, E., Dominguez, J.M., 2nd, Hu, P., Thinschmidt, J.S., Caballero, S., Li Calzi, S., Luo, D., Shanmugam, S., Salazar, T.E., Duan, Y., et al. (2016). CX3CR1 deficiency accelerates the development of retinopathy in a rodent model of type 1 diabetes. J. Mol. Med. (Berl.) *94*, 1255–1265.

46. Grüter, O., Kostic, C., Crippa, S.V., Perez, M.T., Zografos, L., Schorderet, D.F., Munier, F.L., and Arsenijevic, Y. (2005). Lentiviral vector-mediated gene transfer in adult mouse photoreceptors is impaired by the presence of a physical barrier. Gene Ther. *12*, 942–947.

47. Blanks, J.C., Johnson, L.V., and Hageman, G.S. (1993). Stage-specific binding of peanut agglutinin to aggregates of degenerating photoreceptor cells in the rd mouse retina. Exp. Eye Res. *57*, 265–273.

48. Gargini, C., Terzibasi, E., Mazzoni, F., and Strettoi, E. (2007). Retinal organization in the retinal degeneration 10 (rd10) mutant mouse: a morphological and ERG study. J. Comp. Neurol. *500*, 222–238.

49. Silva, M., and Gras, J. (1979). [Conditions for greater survival of neonatally thymectomized Swiss mice (author's transl)]. Rev. Esp. Fisiol. *35*, 85–87.

50. Hirate, J., Horikoshi, I., Watanabe, J., and Ozeki, S. (1984). Effect of hypothermia and ether anesthesia on the dispositions of creatinine and urea in mice. J. Pharmacobiodyn. *7*, 883–890.

51. Liu, S., Li, Z.W., Weinreb, R.N., Xu, G., Lindsey, J.D., Ye, C., Yung, W.H., Pang, C.P., Lam, D.S., and Leung, C.K. (2012). Tracking retinal microgliosis in models of retinal ganglion cell damage. Invest. Ophthalmol. Vis. Sci. *53*, 6254–6262.

52. Ma, W., Cojocaru, R., Gotoh, N., Gieser, L., Villasmil, R., Cogliati, T., Swaroop, A., and Wong, W.T. (2013). Gene expression changes in aging retinal microglia: relationship to microglial support functions and regulation of activation. Neurobiol. Aging *34*, 2310–2321.

53. Peng, B., Xiao, J., Wang, K., So, K.F., Tipoe, G.L., and Lin, B. (2014). Suppression of microglial activation is neuroprotective in a mouse model of human retinitis pigmentosa. J. Neurosci. *34*, 8139–8150.

54. Wang, G., Zhang, J., Hu, X., Zhang, L., Mao, L., Jiang, X., Liou, A.K., Leak, R.K., Gao, Y., and Chen, J. (2013). Microglia/macrophage polarization dynamics in white matter after traumatic brain injury. J. Cereb. Blood Flow Metab. *33*, 1864–1874.

55. Davis, R.J., Tosi, J., Janisch, K.M., Kasanuki, J.M., Wang, N.K., Kong, J., Tsui, I., Cilluffo, M., Woodruff, M.L., Fain, G.L., et al. (2008). Functional rescue of degenerating photoreceptors in mice homozygous for a hypomorphic cGMP phosphodiesterase 6 b allele (Pde6bH620Q). Invest. Ophthalmol. Vis. Sci. *49*, 5067–5076.

56. Hart, A.W., McKie, L., Morgan, J.E., Gautier, P., West, K., Jackson, I.J., and Cross, S.H. (2005). Genotype-phenotype correlation of mouse pde6b mutations. Invest. Ophthalmol. Vis. Sci. *46*, 3443–3450.